Journal of Organometallic Chemistry 693 (2008) 3035–3042

Contents lists available at ScienceDirect

Journal of Organometallic Chemistry

journal homepage: www.elsevier.com/locate/jorganchem

Synthesis, characterization, and structural study of iron–sulfur core $\{Cp_2Fe_2(\mu\text{-}SEt)_2\}$ complexes

Sodio C.N. Hsu [a,*], Yu-Chen Zheng [a], Hsing-Yin Chen [a], Min-Yuan Hung [b], Ting-Shen Kuo [c]

[a] Faculty of Medicinal and Applied Chemistry, and Center of Excellence for Environmental Medicine, Kaohsiung Medical University, Kaohsiung 807, Taiwan
[b] Center for Resources, Research & Development, Kaohsiung Medical University, Kaohsiung 807, Taiwan
[c] Department of Chemistry, National Taiwan Normal University, Taipei 116, Taiwan

ARTICLE INFO

Article history:
Received 24 April 2008
Received in revised form 16 June 2008
Accepted 17 June 2008
Available online 25 June 2008

Keywords:
Iron
Sulfur
Phosphine
Cyanide

ABSTRACT

The known complexes $[Cp_2Fe_2(\mu\text{-}SEt)_2(MeCN)_2](PF_6)_2$ (**1**) and $Cp_2Fe_2(\mu\text{-}SEt)_2(CN)_2$ (**2**) are prepared to investigate their reactivity. The reaction of complex **2** with equimolar amounts of MeOTf yields a monomethylation product $[Cp_2Fe_2(\mu\text{-}SEt)_2(CN)(CNMe)](OTf)$ (**3**). Dimethylation of complex **2** by 2 equiv. MeOTf gives a complex $[Cp_2Fe_2(\mu\text{-}SEt)_2(CNMe)_2](OTf)_2$ (**4**). Complex **1** containing two labile MeCN ligands reacts with several bidentate phosphine ligands, such as dppm, dppa, and dppf, to afford complexes $[Cp_2Fe_2(\mu\text{-}SEt)_2(dppm)](PF_6)_2$ (**5**), $[Cp_2Fe_2(\mu\text{-}SEt)_2(dppa)](PF_6)_2$ (**6**), and $[Cp_2Fe_2(\mu\text{-}SEt)_2(dppf)](PF_6)_2$ (**7**), respectively. The spectroscopic, electrochemical, and reactivity studies of iron–sulfur core complexes are performed. The structures of complexes **1**–**7** were confirmed by X-ray crystallography.

1. Introduction

The chemistry on abiological iron–sulfur complexes has been reviewed [1,2] and regarded to the primordial chemistry of life evolution [3–5]. Iron–sulfur complexes are of significant interest as synthetic analogues for the mimicking the redox behavior of active sites of metalloproteins, such as hydrogenase and ferredoxins [6–8]. The studies on the synthetic model complexes containing iron–sulfur core not only provide a better understanding of the biological molecules but also provide fundamental knowledge in iron–sulfur coordination chemistry, which is necessary for a deeper understanding of iron containing non-heme enzymes. Among synthetic iron–sulfur complexes, dinuclear cyclopentadienyl thiolate-bridged species are a well-established class of compounds [2,9]. A series of studies on the iron–sulfur core $\{Cp_2Fe_2(\mu\text{-}SR)_2\}$ complexes (R = alkyl or aryl), of their redox and/or their crystal structures have reported [10–25]. However, their reactivity has been comparatively little explored [10,16,17]. In this paper, we reported the reactivity of complex $[Cp_2Fe_2(\mu\text{-}SEt)_2(MeCN)_2](PF_6)_2$ (**1**) and its cyanide adduct $Cp_2Fe_2(\mu\text{-}SEt)_2(CN)_2$ (**2**). In addition, the solid state structure and reactivity of these dinuclear cyclopentadienyl thiolate-bridged complexes containing isocyanide or bidentate phosphine ligands were also investigated.

2. Experimental

All manipulations were carried out under an atmosphere of purified dinitrogen with standard Schlenk techniques. Chemical reagents were purchased from Aldrich Chemical Company Ltd., Lancaster Chemicals Ltd., or Fluka Ltd. All the reagents were used without further purification, apart from all solvents that were dried over Na (Et_2O, THF) or CaH_2 (CH_2Cl_2, CH_3CN) and then thoroughly degassed before use.

$[Cp_2Fe_2(\mu\text{-}SEt)_2(CO)_2](PF_6)_2$ were prepared according to the literature procedures [26]. IR spectra were recorded on a Perkin–Elmer System 2000 FT-IR spectrometer. ^1H NMR, ^{13}C NMR and ^{31}P NMR spectra were acquired on a Varian Gemini-200 proton/Carbon FT NMR or a Varian Gemini-500 proton/Carbon FT NMR spectrometer. ESI mass spectra were collected on a Waters ZQ 4000 mass spectrometer. Elemental analyses were performed on a Heraeus CHN-OS Rapid Elemental Analyzer. Cyclic voltammetry were measured at a scan rate of 100 mV/s on 10^{-3} M MeCN solutions using 0.1 M $(Bu_4N)(PF_6)$ as supporting electrolyte and referenced to $Fc^{+/0}$. A platinum wire counter electrode, a glassy carbon working electrode, and an Ag/AgCl (MeCN) reference electrode were used.

2.1. $[Cp_2Fe_2(\mu\text{-}SEt)_2(MeCN)_2](PF_6)_2$ (**1**)

A mixture of 2.3 g (3.24 mmol) of $[Cp_2Fe_2(\mu\text{-}SEt)_2(CO)_2](PF_6)_2$ and 2 g (12.2 mmol) of NH_4PF_6 was refluxed in 70 mL MeCN in a round-bottomed flask with a condenser open to the air. After 6 h

* Corresponding author. Tel.: +886 7 3121101; fax: +886 7 3125339.
E-mail address: sodiohsu@kmu.edu.tw (S.C.N. Hsu).

0022-328X/$ - see front matter © 2008 Elsevier B.V. All rights reserved.
doi:10.1016/j.jorganchem.2008.06.025

refluxing, the mixture was reduced in volume to about 8 mL, and addition of 50 mL of H_2O precipitated the product, $[Cp_2Fe_2(\mu\text{-}SEt)_2(MeCN)_2](PF_6)_2$. The product was washed with 20 mL H_2O. Redissolving the initial product in 70 mL MeCN and reducing solvent slowly in rotavapor to give a pure black microcrystalline product. Yield: 1.48 g (62%). IR (KBr, cm^{-1}): ν_{CN} = 2295(s). ^1H NMR (CD_3CN): δ 1.72 (t, J_{H-H} = 7 Hz, 6H, CH_3CH_2S), 1.95 (s, 6H, $NCCH_3$), 2.45 (quartet, J_{H-H} = 7 Hz, 4H, CH_3CH_2S), 5.33 (s, 10H, C_5H_5). ESI-MS(+): m/z = 223.0 ($[Cp_2Fe_2(\mu\text{-}SEt)_2(NCMe)_2]^{2+}$).

2.2. $[Cp_2Fe_2(\mu\text{-}SEt)_2(CN)_2]$ (**2**)

To a solution of **1** (1.0 g, 1.36 mmol) in 50 mL MeCN was added KCN (0.400 g, 6.16 mmol) dissolved in 50 mL water. The solution was stirred for 10 min under an inert atmosphere. The solvent was evaporated and the residue extracted several times with CH_2Cl_2. The orange-brown solution was taken to dryness and the solid dried under vacuum. Yield: 0.546 g (97%). ^1H NMR ($CDCl_3$): δ 1.60 (t, J_{H-H} = 7.2 Hz, 6H, SCH_2CH_3), 2.79 (quartet, J_{H-H} = 7.2 Hz, 4H, SCH_2CH_3), 5.02 (s, 10H, C_5H_5). ^{13}C NMR ($CDCl_3$): δ 17.03 (s, SCH_2CH_3), 41.17 (s, SCH_2), 88.81 (s, C_5H_5), 175.86 (s, CN). IR (KBr): νCN = 2097(s).

2.3. $[Cp_2Fe_2(\mu\text{-}SEt)_2(CN)(CNMe)](OTf)$ (**3**)

To a solution of **2** (0.020 g, 0.048 mmol) in 5 mL CH_2Cl_2 was added 1 M MeOTf (50 μL, 0.05 mmol) dissolved in THF. The solution was stirred for 5 min under N_2 atmosphere at 0 °C. A yellow solid precipitated on addition of Et_2O. Yield: 0.013 g (48%). ^1H NMR (D_2O): δ 1.50 (t, J_{H-H} = 7.4 Hz, 6H, SCH_2CH_3), 2.71 (quartet, J_{H-H} = 7.4 Hz, 4H, SCH_2CH_3), 3.27 (s, 3H, $CNCH_3$), 5.34 and 5.28 (s, 10H, C_5H_5). ^{13}C NMR (D_2O): δ 16.31 (s, SCH_2CH_3), 30.63 (s, $CNCH_3$) 40.45 (s, SCH_2), 90.47, 90.54 (s, C_5H_5), 145.51 (s, $CNMe$), 152.42 (s, CN), CF_3SO_3- not observed. IR (KBr): νCNMe = 2212(s), νCN = 2101 (w), IR (CH_3CN): νCNMe = 2205(s), νCN = 2108 (w), ESI-MS(+): m/z = 431.1 ($[Cp_2Fe_2(\mu\text{-}SEt)_2(CN)(CNMe)]^+$). Anal. Calc. for $C_{18}H_{23}F_3Fe_2N_2O_3S_3 \cdot THF_{1/4}$: C, 38.21; H, 4.05; N, 4.69. Found: C, 38.19; H, 4.17; N, 5.02%.

2.4. $[Cp_2Fe_2(\mu\text{-}SEt)_2(CNMe)_2](OTf)_2$ (**4**)

Method A: To a solution of **2** (0.020 g, 0.048 mmol) in 5 mL CH_2Cl_2 was added 1 M MeOTf (2 mL, 2 mmol) dissolved in THF. The solution was stirred for 3 h under N_2 atmosphere. Microcrystal **4** was collected on a glass frit and dried under vacuum. Yield: 0.028 g (79%). ^1H NMR (D_2O): δ 1.54 (t, J_{H-H} = 7.2 Hz, 6H, SCH_2CH_3), 2.73 (quartet, J_{H-H} = 7.4 Hz, 4H, SCH_2CH_3), 3.33 (s, 6H, $CNCH_3$), 5.50 (s, 10H, C_5H_5). ^{13}C NMR (D_2O): δ 16.33 (s, SCH_2CH_3), 31.00 (s, $CNCH_3$), 41.67 (s, SCH_2), 91.66 (s, C_5H_5), 118 (t, J_{C-F} = 315.4 Hz, OTf), 142.43 (s, $CNMe$). IR (KBr): νCNMe = 2227(s), ESI-MS(+): m/z = 223.1 ($[Cp_2Fe_2(\mu\text{-}SEt)_2(CNMe)_2]^{2+}$), 595.2 ($\{[Cp_2Fe_2(\mu\text{-}SEt)_2(CNMe)_2][OTf]\}^+$). Anal. Calc. for $C_{20}H_{26}F_6Fe_2N_2O_6S_4 \cdot 0.5CH_2Cl_2$: C, 31.29; H, 3.46; N, 3.56. Found: C, 31.05; H, 3.56; N, 3.60%.

Method B: A solution of 1 (0.090 g, 0.12 mmol) and MeNC (66 μL, 10 equiv.) in 20 mL acetone was stirred for 24 h under N_2 atmosphere. The solvent was evaporated under vacuum and the residue washed with CH_2Cl_2. The solution was filtered and the solid was dried under vacuum. Yield: 0.055 g (77%).

2.5. $[Cp_2Fe_2(\mu\text{-}SEt)_2(dppm)](PF_6)_2$ (**5**)

A mixture of **1** (0.095 g, 0.13 mmol) and dppm (0.050 mg, 0.13 mmol) were dissolved in 30 mL of acetone under N_2 atmosphere. After stirring for 48 h, the color of mixture is darker. The reaction mixture was evaporated to dryness, and the residue was redissolved in 20 mL of CH_2Cl_2 and filtered, while the reactant **1** did not dissolve in CH_2Cl_2. The filtrate was reduced to ca. 5 mL under vacuum then 20 mL of Et_2O was added to precipitate the dark green product. Yield: 130 mg (97%). ^1H NMR (CD_3CN): δ 1.63 (t, J_{H-H} = 7.6 Hz, 6H, CH_3CH_2S), 2.35 (t, J_{H-H} = 11.6 Hz, 2H, CH_2 of dppm), 3.35 (quartet, 4H, J_{H-H} = 7.2 Hz, CH_3CH_2S), 5.39 (s, 10H, C_5H_5), 7.24–7.68 (m, 20H, Ph). ^{31}P NMR(CD_3CN): δ 50.51 (s, dppm), −145.64 (quint., PF_6), ESI-MS(+): m/z = 374.8 ($[Cp_2Fe_2(\mu\text{-}SEt)_2(dppm)]^{2+}$). Anal. Calc. for $C_{39}H_{42}F_{12}Fe_2P_4S_2$: C, 45.11; H, 4.08. Found: C, 45.07; H, 4.11%.

2.6. $[Cp_2Fe_2(\mu\text{-}SEt)_2(dppa)](PF_6)_2$ (**6**)

A mixture of **1** (0.090 g. 0.12 mmol) and dppa (0.050 g 0.13 mmol) were dissolved in 30 mL of acetone under N_2 atmosphere. After stirring for 48 h, the color of mixture is darker. The reaction mixture was evaporated to dryness, and the residue was redissolved in 20 mL of CH_2Cl_2 and filtered. The filtrate was reduced to ca. 5 mL under vacuum then 20 mL of Et_2O was added to precipitate the dark green product. Yield: 110 mg (92%). ^1H NMR (acetone-d_6): δ 1.73 (t, J_{H-H} = 7.2 Hz, 6H, CH_3CH_2S), 3.75 (quartet, 4H, J_{H-H} = 7.2 Hz, CH_3CH_2S), 5.38 (t, J_{H-H} = 8.8 Hz, 1H, NH of dppa), 5.85 (s, 10H, C_5H_5), 7.49–7.66 (m, 20H, Ph). ^{13}C NMR (acetone-d_6): δ 18.20 (s, SCH_2CH_3), 47.66 (s, SCH_2CH_3), 94.16 (s, C_5H_5), 130.20–133.98 (m, Ph). ^{31}P NMR (acetone-d_6): δ 99.00 (s, dppa), −146.29 (quint., PF_6), IR (KBr): νN–H = 3118. ESI-MS(+): m/z = 374.3 ($[Cp_2Fe_2(\mu\text{-}SEt)_2(dppa)]^{2+}$). Anal. Calc. for $C_{38}H_{41}F_{12}Fe_2N_1P_4S_2 \cdot 0.5CH_2Cl_2$: C, 42.74; H, 3.91; N, 1.29. Found: C, 42.98; H, 4.26; N, 1.22%.

2.7. $[Cp_2Fe_2(\mu\text{-}SEt)_2(dppf)](PF_6)_2$ (**7**)

A mixture of **1** (0.070 g, 0.10 mmol) and dppf (0.060 g, 0.11 mmol) were dissolved in 30 mL of acetone under N_2 atmosphere. After stirring for 48 h, the reaction mixture was evaporated to dryness, and the residue was redissolved in 20 mL of CH_2Cl_2 and filtered. The filtrate was reduced to ca. 5 mL under vacuum then 20 mL of Et_2O was added to precipitate the brown product. Yield: 65 mg (40%). ^1H NMR (acetone-d_6): δ 1.11 (t, J_{H-H} = 6.8 Hz, 6H, CH_3CH_2S), 3.40 (quartet, 4H, J_{H-H} = 6.8 Hz, CH_3CH_2S), 4.52 and 4.73 (s, 8H, Cp of dppf), 5.75 (s, 10H, C_5H_5), 7.67–7.93 (m, 20H, Ph). ^{31}P NMR (acetone-d_6): δ 30.49 (s, dppf), −143.18 (quint., PF_6). ESI-MS(+): m/z = 459.2 ($[Cp_2Fe_2(\mu\text{-}SEt)_2(dppf)]^{2+}$). Anal. Calc. for $C_{48}H_{48}F_{12}Fe_3P_4S_2$: C, 47.71; H, 4.00. Found: C, 47.86; H, 4.30%.

2.8. X-ray structural analysis

Single crystals suitable for X-ray analysis of complexes **1**, **5**, **6** were obtained by diffusion of ether into CH_3CN solution. For crystal sample of complexes **2**, **3**, **4**, **7** were obtained by diffusion of Et_2O into acetone solution. All single-crystal X-ray diffraction data were measured on a Bruker Nonius Kappa CCD diffractometer using λ (Mo Kα) radiation (λ = 0.71073 Å). The data collection was executed using the SMART program. Cell refinement and data reduction were made with the SAINT program. The structure was determined using the SHELXTL/PC program and refined using full-matrix least-squares. All non-hydrogen atoms were refined anisotropically, whereas hydrogen atoms were placed at the calculated positions and included in the final stage of refinements with fixed parameters. A summary of relevant crystallographic data for complexes **1**–**7** is provided in Table 1.

3. Results and discussion

Treatment of $[Cp_2Fe_2(\mu\text{-}SEt)_2(NCMe)_2](PF_6)_2$ (**1**) with 2 equiv. of the KCN result in the formation of the neutral cyanide adducts complex $Cp_2Fe_2(\mu\text{-}SEt)_2(CN)_2$ (**2**) in essentially quantitative yields.

Table 1
Crystallographic data for iron–sulfur core complexes **1**, **2**, **3**, **4**, **5**, **6** and **7**

	1	**2**	**3**	**4**	**5** · 1.5NCMe	**6** · NCMe	**7**
Empirical formula	$C_{18}H_{26}F_{12}Fe_2N_2P_2S_2$	$C_{16}H_{20}Fe_2N_2S_2$	$C_{18}H_{23}F_3Fe_2N_2O_3S_3$	$C_{20}H_{26}F_6Fe_2N_2O_6S_4$	$C_{84}H_{93}F_{24}Fe_4N_3P_8S_4$	$C_{40}H_{44}F_{12}Fe_2N_2P_4S_2$	$C_{48}H_{48}F_{12}Fe_3P_4S_2$
Formula weight	736.17	416.16	580.26	744.37	2200.01	1080.47	1208.41
T (K)	200(2)	200(2)	200(2)	200(2)	150(2)	200(2)	100(2)
Crystal size (mm^3)	0.2 × 0.09 × 0.03	0.21 × 0.11 × 0.02	0.28 × 0.15 × 0.07	0.38 × 0.2 × 0.08	0.26 × 0.15 × 0.09	0.24 × 0.14 × 0.04	0.15 × 0.10 × 0.04
Crystal system	Orthorhombic	Orthorhombic	Monoclinic	Monoclinic	Triclinic	Orthorhombic	Orthorhombic
Space group	$P2_1mn$	$Pcab$	$C2/c$	$P2_1/c$	$P\bar{1}$	$Pnan$	$Pbcn$
a (Å)	12.1244(12)	15.5341(7)	24.0327(6)	11.6578(5)	16.0882(2)	13.0397(5)	14.9075(9)
b (Å)	10.0827(10)	15.3085(7)	10.3123(2)	15.5137(6)	16.3991(2)	17.9504(8)	15.9513(10)
c (Å)	10.9801(12)	28.3557(13)	19.0380(6)	16.9204(7)	18.6519(2)	19.5170(11)	19.6302(12)
α (°)	90	90	90	90	92.1630(10)	90	90
β (°)	90	90	101.6850(10)	109.399(2)	107.0340(10)	90	90
γ (°)	90	90	90	90	96.92	90	90
V ($Å^3$)	1342.3(2)	6743.1(5)	4620.5(2)	2886.4(2)	4656.99(10)	4568.3(4)	4667.9(5)
Z	2	16	8	4	2	4	4
D_{calcd} (g cm^{-3})	1.821	1.640	1.668	1.713	1.569	1.571	1.719
μ (mm^{-1})	1.452	1.965	1.574	1.372	0.931	0.948	1.232
Reflections measured/ independent	8137/1318	40662/5976	15709/4186	16435/5245	69252/17012	19503/4154	34293/4114
Data/restraints/ parameters	1318/0/102	5976/0/385	4186/0/282	5245/0/361	17012/0/1145	4154/0/281	4114/0/312
Goodness-of-fit	1.035	1.111	1.112	1.007	1.069	1.090	1.051
R_{int}	0.0971	0.0972	0.0753	0.0641	0.0724	0.1793	0.0796
R_1 [$I > 2\sigma$] (all data)	0.0867 (0.1305)	0.0412 (0.0766)	0.0583 (0.0866)	0.0422 (0.0668)	0.0540 (0.0833)	0.0957 (0.1892)	0.0317 (0.0558)
R_w [$I > 2\sigma$] (all data)	0.2419 (0.2859)	0.0801 (0.0910)	0.1403 (0.1812)	0.1088 (0.1282)	0.1422 (0.1794)	0.2089 (0.2699	0.0661 (0.0746)
Maximum peak/ hole ($e^-/Å^3$)	1.652/−1.496	1.090/−0.909	1.240/−1.413	0.555/−0.819	1.307/−1.228	1.472/−0.804	0.443/−0.552

The reaction of **2** with 1 equiv. of methyl trifluoromethanesulfonate (MeOTf) produce the monomethylated yellow salt [Cp_2Fe_2-(μ-SEt)$_2$(CN)(CNMe)](OTf) (**3**). The dimethylation product [Cp_2Fe_2(μ-SEt)$_2$(CNMe)$_2$](OTf)$_2$ (**4**) can be obtained as the exclusive product by the reaction of **2** with 2 equiv. of the MeOTf or directly perform the reaction of **1** with methyl isocyanide (Scheme 1). The ESI-MS(+) spectrometry data of complexes **1**, **3** and **4** show the molecular ion peaks and their corresponding fragment ion peaks, which lose coordinated MeCN or methyl isocyanide ligands. The IR νCN at 2295 cm^{-1}(w) for **1**, 2097 cm^{-1}(s) for **2**, and 2227 cm^{-1}(s) observed for **4** also suggests the presence of a coordinated MeCN, cyanide and methyl isocyanide, respectively, which are consistent with the X-ray structure results. The IR νCN at 2101 cm^{-1}(s) and 2212 cm^{-1}(s) for **3** show the both cyanide and isocyanide features (Fig. 1). The ^{1}H and ^{13}C{^{1}H} NMR spectra of **1**, **2** and **4** exhibit sharp lines indicating their diamagnetic nature; i.e., the presence of a Fe–Fe single bond. Complexes **1**, **2** and **4** give rise to only one set of Cp signals in the range 5.0–6.0 ppm and the ethylthiolate proton resonances around 2.6(q) and 1.3(t) ppm in the ^{1}H NMR spectrum. The proton resonance of the MeCN ligands for **1** gives a singlet at 1.95 ppm and the CNMe ligands for **4** also gives a singlet at 3.59 ppm. On the other hand, the ^{1}H NMR spectrum of **3** shows one CN*Me* singlet, two Cp singlets and the ethylthiolate proton resonances, consistent with the low symmetry of **3** compared with **1**, **2** and **4**. The ^{13}C{^{1}H} NMR spectrum of **3** also shows two signals in the *C*N region and two Cp signals, consistent with the low symmetry of this complex compared with **4** (see above).

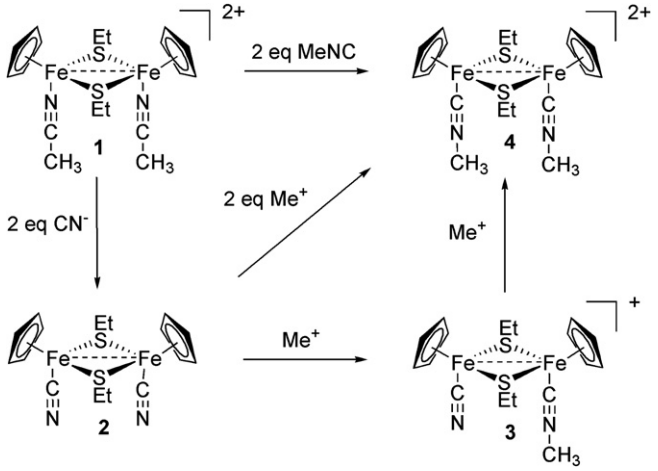

Scheme 1.

It is noticed that Kubas and Vergamini had reported complexes **1** and **2** [16,17]. We report the crystallography results of complexes **1** and **2** here for comparison with complex **3** and **4** in molecular structural data. The solid-state structures of **1**, **2**, **3** and **4** were determined by single-crystal X-ray diffraction, confirming their dinuclear nature. Only complex **2** displayed two similar molecules of Cp_2Fe_2(μ-SEt)$_2$(CN)$_2$ in the asymmetric unit, which is distinct from literature result [17]. ORTEP plots of **1**, **2**, **3** and **4** are depicted in Figs. 2–5, respectively. Selected bond distances and angles are reported in Table 2.

Complexes **1**, **2**, **3** and **4** all contain two CpFe units in a mutually *cis* configuration bridged by two ethylthiolate ligands with the substituents adopting a *syn* orientation with respect to one another but *anti* with respect to the Cp ligands. The MeCN, CN, or CNMe ligands occupy the remaining coordination sites. The dihedral angles between the two FeSFe planes are 167.9 for **1**, 154.6 for **2**, 157.70 for **3**, and 154.6 for **4**. Similar structural features are observed for the related thiolate-bridged CpFe complexes **1** and **2** that have been reported [17], but we could not find out their detail crystallography data in CSD database. The Fe–S distances in the range 2.17–2.26 Å are comparable to those of other thiolate-bridged diiron centers with Fe(III) centers [10,17]. The Fe–Fe distances of **1**, **2**, **3** and **4** of 2.638(2), 2.6315(9), 2.6372(10) and 2.6467(8) Å, respectively, agree well with comparable values for [Cp_2Fe_2(μ-SEt)$_2$(NCMe)$_2$]$^{2+}$ and other related complexes [10,17]; they fall in the 2.5–2.8 Å range which are characteristic of two-electron Fe–Fe bond [10,17].

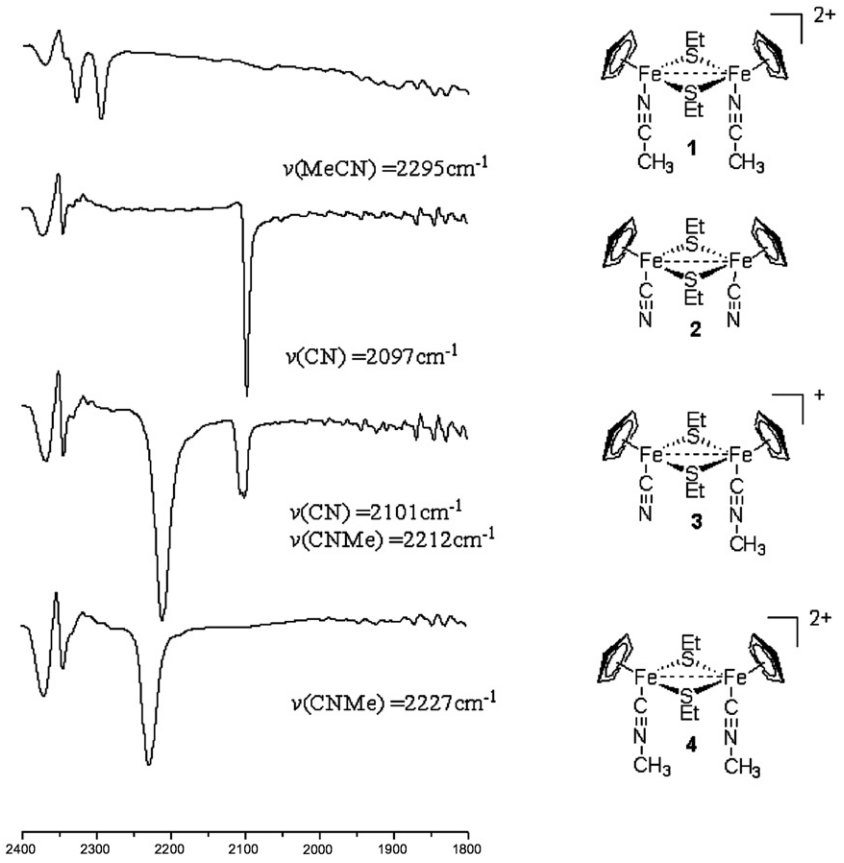

Fig. 1. Solid-state FT-IR spectra (KBr) of **1**, **2**, **3** and **4**.

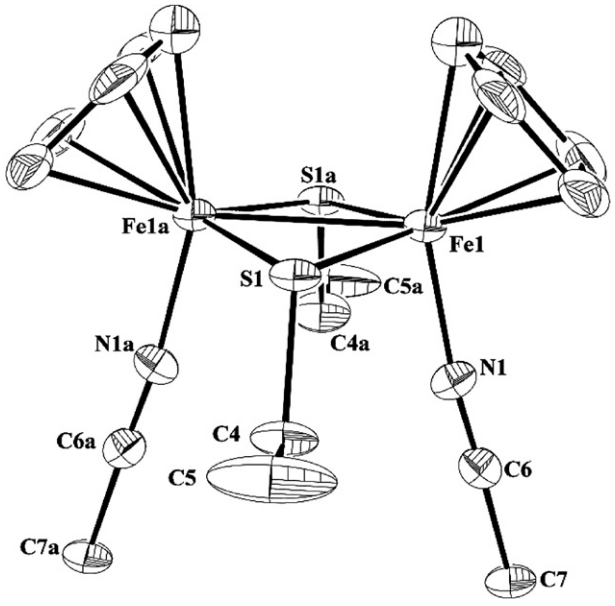

Fig. 2. ORTEP representation of the crystal structures of the cation of $Cp_2Fe_2(\mu\text{-}SEt)_2(MeCN)_2](PF_6)_2$ (**1**).

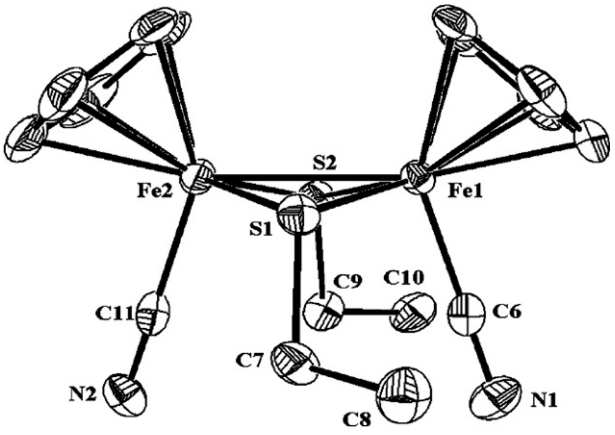

Fig. 3. ORTEP representation of the crystal structures of the cation of $Cp_2Fe_2(\mu\text{-}SEt)_2(CN)_2](PF_6)_2$ (**2**).

The substitutionally labile acetonitrile ligands in complex **1** are readily replaced by diphosphine ligands (Scheme 2). Thus, the synthesis of complex $[Cp_2Fe_2(\mu\text{-}SEt)_2(\mu\text{-}dppm)](PF_6)_2$ (**5**) become accessible by reaction of complex **1** and dppm. In a similar fashion, the reaction of dppa or dppf and **1** yield the complexes $[Cp_2Fe_2(\mu\text{-}SEt)_2(\mu\text{-}dppa)](PF_6)_2$ (**6**) or $[Cp_2Fe_2(\mu\text{-}SEt)_2(\mu\text{-}dppf)](PF_6)_2$ (**7**), respectively. All these complexes are air-stable solids. Characterization was afforded by elemental analysis and ^1H and $^{31}P\{^1H\}$ NMR spectroscopy. The ESI-MS(+) spectrometry data of complexes **5**, **6** and **7** exhibit their well-resolved molecular ion peaks.

Complexes **5**, **6** and **7** have also been characterized by X-ray crystallography. Structural views are shown in Figs. 6–8. Selected bond distances and angles are summarized in Table 3. Complex **5** also displayed two similar molecules in the asymmetric unit. Complexes **5**, **6** and **7** contain two CpFe units in a mutually cis configuration bridged by two thiolate ligands, with the ethylthiolate substituents adopting a syn orientation with respect to one another. In contrast to **1**, **2** and **4**, the ethylthiolate substituents are

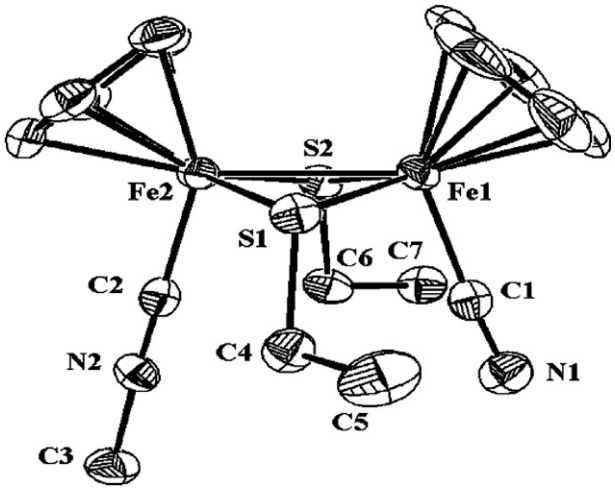

Fig. 4. ORTEP representation of the crystal structures of the cation of $Cp_2Fe_2(\mu\text{-}SEt)_2(CN)(CNMe)(OTf)$ **(3)**.

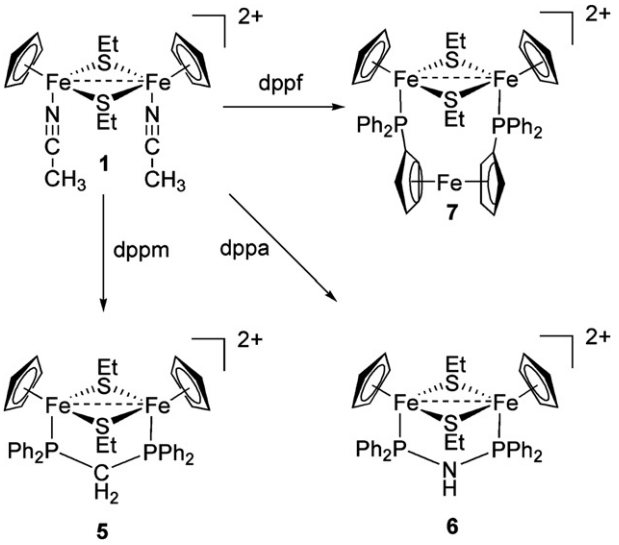

Scheme 2.

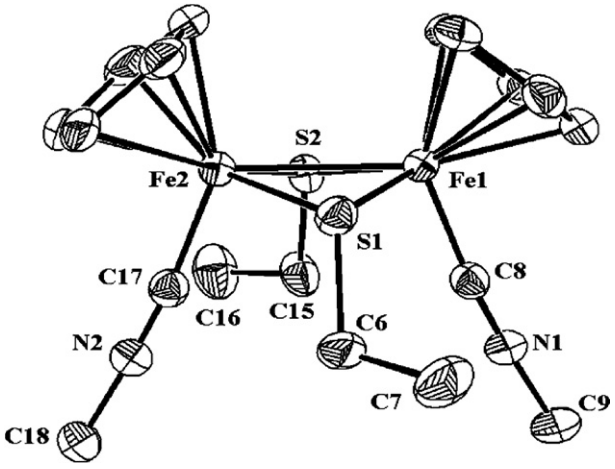

Fig. 5. ORTEP representation of the crystal structures of the cation of $[Cp_2Fe_2(\mu\text{-}SEt)_2(CNMe)_2]$ **(4)**.

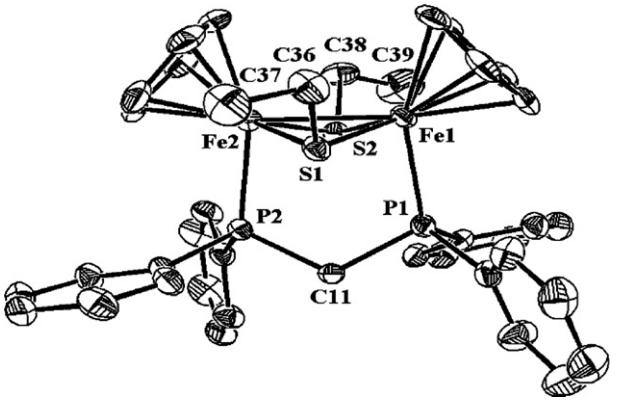

Fig. 6. ORTEP representation of the crystal structures of the cation of $[Cp_2Fe_2(\mu\text{-}SEt)_2(\mu\text{-}dppm)]$ **(5)**.

syn oriented with respect to the Cp ligands. The remaining coordination sites of **5**, **6** and **7** are occupied by a bridging dppm, dppa or dppf ligands. The different orientations of ethylthiolate substituents on bridging sulfur atoms between complexes **1**–**4** and **5**–**7** are due to steric effect of diphenyl phosphine moiety of diphosphine ligands. The Fe–Fe distances of 2.6544(9) and 2.631(2) Å for of complexes **5** and **6**, respectively, clearly indicates the presence of a metal–metal single bond. The Fe–Fe distance of adduct **7** is longer than those of **5** and **6** also exhibits a metal–metal single bond character. The longer Fe–Fe bond in **7**, which expand the Fe–Fe distance to 2.7279(8) Å, suggests the dppf ligand has large bite angle compared to dppm and dppa ligand.

Table 2
Selected bond lengths and angles of **1**, **2**, **3**, and **4** and other relevance Fe_2S_2 core complexes

Complexes		Fe–Fe	S–Fe–S	Fe–S–Fe	Fe–S	Ref.
$Cp_2Fe_2(\mu\text{-}SEt)_2(CO)_2$	Molecule 1	3.450(2)	79.2(1)	99.1(1)	2.262(2), 2.271(3)	[13]
	Molecule 2	3.415(2)	81.1(1)	97.2(1)	2.274(3), 2.279(2)	
$[Cp_2Fe_2(\mu\text{-}SEt)_2(CO)_2]^+$		2.957(4)	95.7(2)	82.8(2)	2.240(2)	[15]
$[Cp_2Fe_2(\mu\text{-}SEt)_2(NCMe)_2]^{2+}$		2.649(7)	105.2(3)	73.9(3)		[17]
$[Cp_2Fe_2(\mu\text{-}SEt)_2(CN)_2]$		2.625(3)	102.9(2)	73.3(2)		[17]
$[Cp_2Fe_2(\mu\text{-}SEt)_2(NCMe)_2]^{2+}$ $\mathbf{1}^{2+}$		2.638(3)	105.99(12)	73.16(12)	2.214(3), 2.214(3)	This work
$[Cp_2Fe_2(\mu\text{-}SEt)_2(CN)_2]$ **2**	Molecule 1	2.6115(8)	103.37(5), 103.27(5)	73.06(4), 73.19(4)	2.1803(12), 2.2071(13) 2.1753(11), 2.2050(13)	This work
	Molecule 2	2.6515(9)	102.52(5), 102.81(5)	73.74(4), 73.63(4)	2.1994(13), 2.2333(13) 2.1999(13), 2.2249(14)	
$[Cp_2Fe_2(\mu\text{-}SEt)_2(CN)(CNMe)]^+$ $\mathbf{3}^+$		2.6372(10)	103.85(5), 103.53(5)	73.43(4), 73.49(5)	2.2016(15), 2.2032(13) 2.2066(13), 2.2079(14)	This work
$[Cp_2Fe_2(\mu\text{-}SEt)_2(CNMe)_2]^{2+}$ $\mathbf{4}^{2+}$		2.6467(8)	102.49(4), 102.80(4)	73.66(4), 73.75(4)	2.1996(11), 2.2068(12) 2.2086(11), 2.2110(11)	This work

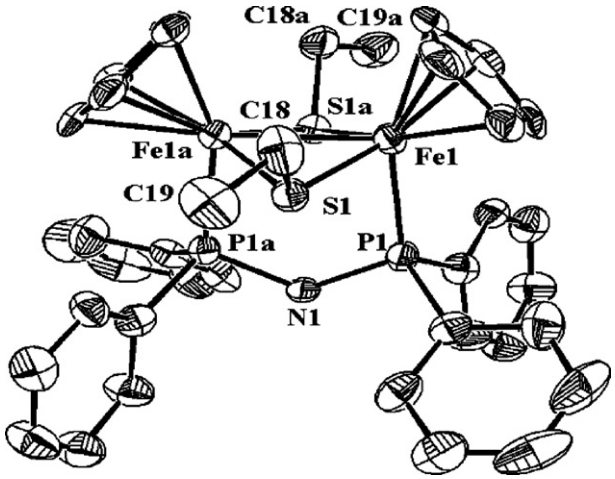

Fig. 7. ORTEP representation of the crystal structures of the cation of $[Cp_2Fe_2(\mu\text{-}SEt)_2(\mu\text{-}dppa)](PF_6)_2$ **(6)**.

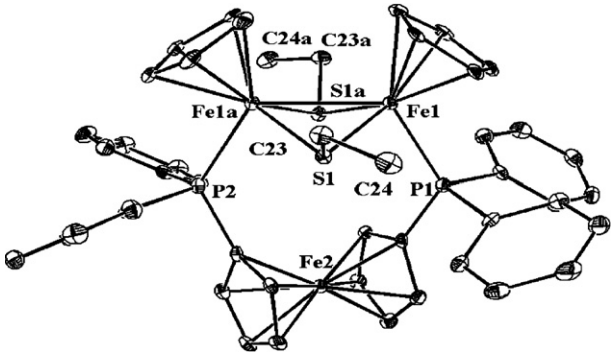

Fig. 8. ORTEP representation of the crystal structures of the cation of $[Cp_2Fe_2(\mu\text{-}SEt)_2(\mu\text{-}dppf)](PF_6)_2$ **(7)**.

Structural characterization and comparison of complexes **1**–**7** and other known iron–sulfur core $\{Cp_2Fe_2(\mu\text{-}SR)_2\}$ complexes clearly illustrate the Fe–Fe distance reveals different iron oxidation states, which are also paralleled by both a substantial drop in the Fe–Fe distance and large distortion angles of Fe–S–Fe, as exemplified in Scheme 3. In fact, the longer Fe–Fe bond lengths are found in paramagnetic $[Cp_2Fe_2(\mu\text{-}SR)_2(CO)_2]^+$ cations for which a one-electron Fe–Fe bond is proposed [15,23]; this lengthening is accompanied by an increase (of ca. 9°) in the Fe–S–Fe angles. Still longer non-bonded Fe–Fe distances of 3.4 Å are found in the comparable iron(II) complexes and are accommodated by a further ca. 16° opening of the Fe–S–Fe angles to 97–100° (Table 2). These findings can be rationalized the occupation of the σ-antibonding orbital of the $(Fe^{III}S)_2$ core by one and two electrons or explained by in turn of removal of electrons from the σ-antibonding of $(Fe^{II}S)_2$ complexes [27].

In order to understand the metal–metal features more detail, the redox properties of **1**–**7** were examined by cyclic voltammetry in acetonitrile. The reduction of iron complexes **1**–**7** are reversible in the first redox step, suggesting that no significant structural reorganization occurs during the redox process. These reversible and quasi-reversible redox waves can be ascribed to electrode processes in the following equations:

$$[Fe^{III}Fe^{III}] + e^- \rightleftharpoons [Fe^{III}Fe^{II}] \quad (1a)$$

$$[Fe^{III}Fe^{II}] + e^- \rightleftharpoons [Fe^{II}Fe^{II}] \quad (1b)$$

$$[Fe^{III}Fe^{III}] + [Fe^{II}Fe^{II}] \overset{K_{com}}{\rightleftharpoons} 2[Fe^{III}Fe^{II}] \quad (2)$$

Similar electrochemical study results are also observed for the related thiolate-bridged CpFe complexes [10,17]. By using the $E_{1/2}$ values for the two redox couples, a comproportionation constant, K_{com}, for the iron–sulfur core $\{Cp_2Fe_2(\mu\text{-}SEt)_2\}$ complexes were calculated according to the equilibrium in Eq. (2) (Table 4). The larger value of K_{com} suggests that the mixed-valence iron radical cation species are quite stable thermodynamically. Indeed, several mixed-valence iron radical complexes containing iron–sulfur core $\{Cp_2Fe_2(\mu\text{-}SR)_2\}$ were reported and studied their one-electron metal–metal bond character [11,21,23,28].

These thiolate-bridged CpFe complexes mostly exhibit third redox couple at comparably high potential area than the other two redox couples (complex **5** as an example shown in Fig. 9), which do not be reported before. This result indicates that the formation of $Fe^{III}Fe^{IV}$ species during the redox process on the electrochemical time scale of thiolate-bridged CpFe complexes. We are not able to isolate the $Fe^{III}Fe^{IV}$ species in pure form. Therefore, we performed density functional theory calculations to characterize the nature of the species. Three different exchange-correlation functionals, including pure functionals BLYP and PBE and hybrid functional B3LYP, were used in combination with medium-sized 6-31G(d)

Table 3
Selected bond lengths and angles of **5**, **6**, and **7**

Complexes		Fe–Fe	S–Fe–S	Fe–S–Fe	Fe–S	Fe–P
$[Cp_2Fe_2(\mu\text{-}SEt)_2(dppm)]^{2+}$ $\mathbf{5}^{2+}$	Molecule 1	2.6555(9)	101.19(5), 101.17(5)	73.74(4), 74.46(4)	2.1953(13), 2.2118(13)	2.2494(13)
					2.1937(12), 2.2141(14)	2.2558(13)
	Molecule 2	2.654(9)	100.05(5), 100.41(5)	73.74(4), 74.13(4)	2.2065(13), 2.2135(14)	2.2631(12)
					2.1978(14), 2.2104(13)	2.2537(13)
$[Cp_2Fe_2(\mu\text{-}SEt)_2(dppa)]^{2+}$ $\mathbf{6}^{2+}$		2.631(2)	102.60(9)	72.79(9)	2.214(3), 2.219(3)	2.233(2)
$[Cp_2Fe_2(\mu\text{-}SEt)_2(dppf)]^{2+}$ $\mathbf{7}^{2+}$		2.7279(8)	90.59(3)	75.59(3)	2.2307(9), 2.2208(8)	2.3280(8)

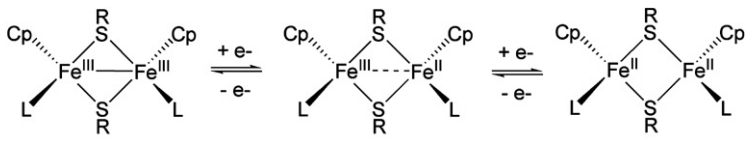

Fe-Fe distance: ~2.6 A ~2.9 A ~3.4 A

L = CO, CN, MeCN, PR_3...

Scheme 3.

Table 4
CV data and comproportionation constant for iron–sulfur core complexes in MeCN–$[NBu_4][PF_6]$[a]

Complex	$E^{ox}_{1/2}$	$E^{Red1}_{1/2}$	$E^{Red2}_{1/2}$	ΔE[c]	K_{com}[d]
$[Cp_2Fe_2(\mu\text{-SR})_2(MeCN)_2](PF_6)_2$ (**1**)	1.361(irr)	−0.605	−1.028(irr)		
$Cp_2Fe_2(\mu\text{-SEt})_2(CN)_2$(**2**)	0.691	−1.196	−1.993(irr)		
$[Cp_2Fe_2(\mu\text{-SEt})_2(CN)(CNMe)](OTf)$(**3**)	1.005	−0.836	−1.545	0.709	9.92×10^{11}
$[Cp_2Fe_2(\mu\text{-SEt})_2(CNMe)_2](OTf)_2$ (**4**)	1.434[b]	−0.525	−1.164	0.639	6.49×10^{10}
$[Cp_2Fe_2(\mu\text{-SEt})_2(dppm)](PF_6)_2$ (**5**)	1.136	−0.634	−1.228	0.594	1.12×10^{10}
$[Cp_2Fe_2(\mu\text{-SEt})_2(dppa)](PF_6)_2$ (**6**)	1.150[b]	−0.627	−1.173	0.546	1.73×10^{9}
$[Cp_2Fe_2(\mu\text{-SEt})_2(dppf)](PF_6)_2$ (**7**)	1.252(irr)[e]	−0.530	−0.978[b]	0.448	3.81×10^{7}

[a] Potentials (in V vs. Fc^+–Fc) were measured at a glassy carbon electrode at a scan rate of 0.1 V s^{-1}.
[b] Quasi-reversible.
[c] $\Delta E = E^{Red1}_{1/2} - E^{Red2}_{1/2}$.
[d] $\Delta E = 0.0591 \log K_{com}$.
[e] Redox potential for dppf at complex **7** = 0.236 V.

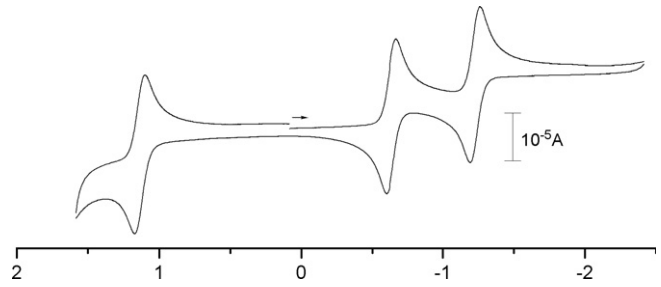

Fig. 9. CV diagram of **5** in MeCN (1×10^{-3} M). Scan rate = 100 mV/s, electrolyte = $(Bu_4N)(PF_6)$ (0.1 M).

basis set in this work. Geometry optimizations for complexes $\mathbf{5}^+$, $\mathbf{5}^{2+}$, and $\mathbf{5}^{3+}$ were carried out and subsequent vibrational frequency analyses were performed to verify that all the optimized geometries are equilibrium structures. Selected optimized geometry parameters for complex **5** at different oxidation states are tabulated in Table 5, and the frontier orbitals of complex $\mathbf{5}^{2+}$ are depicted in Fig. 10.

Regarding complex $\mathbf{5}^{2+}$, geometry parameters predicted by three DFT methods are similar with the PBE results being closest to the crystal data (cf. Table 2 and 5). When going from $\mathbf{5}^{2+}$ to $\mathbf{5}^+$, the most significant geometry change is an increase of Fe–Fe bond length accompanied by a decrease of S–Fe–S angle and an increase of Fe–S–Fe angle. However, comparing theoretical results of $\mathbf{5}^+$ with the crystal data of analogue $[Cp_2Fe_2(\mu\text{-SEt})_2(CO)_2]^+$ reveals that the PBE result is once again most reliable among the three functionals; the Fe–Fe distance of $\mathbf{5}^+$ was estimated to be 3.080 Å, slightly longer than 2.957 Å in $[Cp_2Fe_2(\mu\text{-SEt})_2(CO)_2]^+$ but still in a reasonable value expected for 0.5 bond order. The most significant deviation occurs in the B3LYP calculations, which predict 3.396 Å for Fe–Fe distance. The BLYP results are in between those of B3LYP and PBE. The elongation of Fe–Fe bond upon reduction can be rationalized by the characteristic of LUMO of $\mathbf{5}^{2+}$. The LUMO of $\mathbf{5}^{2+}$ is mainly characterized by Fe–Fe σ-antibonding features. Since the LUMO is the orbital that will be filled by an extra

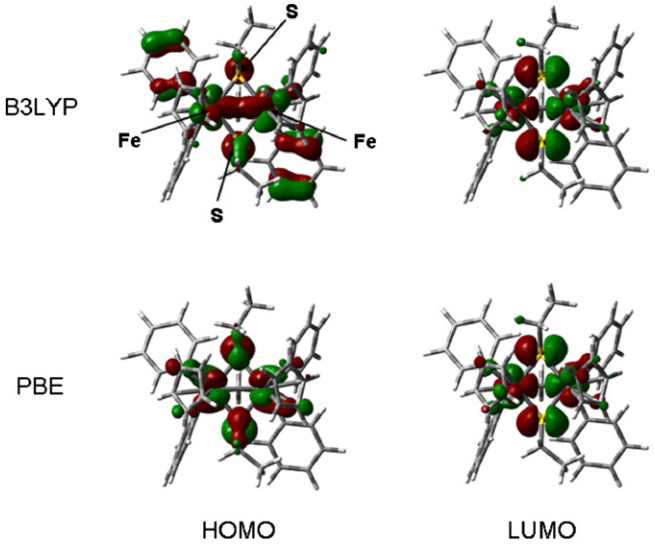

Fig. 10. Frontier orbitals of $[Cp_2Fe_2(\mu\text{-SEt})_2(\mu\text{-dppm})]^{2+}$ ($\mathbf{5}^{2+}$).

electron when the complex is reduced, the Fe–Fe σ-antibonding feature implies that upon reduction the bonding character between iron atoms will be reduced, and thus, leading to the increase of Fe–Fe bond length.

Considering the oxidation of $\mathbf{5}^{2+}$, pure and hybrid DFT calculations displayed very different results. While the hybrid B3LYP method showed a significant increase of Fe–Fe distance from 2.639 to 3.409 Å upon oxidizing $\mathbf{5}^{2+}$ to $\mathbf{5}^{3+}$, this distance was only slightly increased in the pure BLYP (from 2.723 to 2.782 Å) and PBE (from 2.651 to 2.689 Å) calculations. This variations can be attributed to the distinct nature of HOMO predicted by different DFT methods. The B3LYP calculations predicted a strong Fe–Fe σ-bonding feature in the HOMO of $\mathbf{5}^{2+}$; as a consequence, taken an electron away from this orbital (i.e., oxidation) would substantially

Table 5
Selected optimized bond lengths and angles of complex **5** predicted by DFT calculations

Method	Complex	Fe–Fe	S–Fe–S	Fe–S–Fe	Fe–S	Fe–P
B3LYP/6-31G(d)	$\mathbf{5}^+$	3.396	84.1, 88.7	93.0, 93.6	2.273–2.385	2.256, 2.323
	$\mathbf{5}^{2+}$	2.639	102.0, 101.7	72.4, 72.8	2.221–2.238	2.331, 2.343
	$\mathbf{5}^{3+}$	3.409	83.8, 83.2	93.4, 99.5	2.228–2.352	2.359, 2.397
BLYP/6-31G(d)	$\mathbf{5}^+$	3.225	90.3, 90.9	87.4, 88.5	2.299–2.335	2.280, 2.286
	$\mathbf{5}^{2+}$	2.723	100.4, 100.9	74.1, 74.5	2.245–2.264	2.340, 2.352
	$\mathbf{5}^{3+}$	2.782	99.1, 100.0	76.0, 78.0	2.201–2.266	2.388, 2.406
PBE/6-31G(d)	$\mathbf{5}^+$	3.080	91.1, 91.5	85.2, 86.2	2.245–2.276	2.225, 2.232
	$\mathbf{5}^{2+}$	2.651	99.8, 100.1	73.4, 73.8	2.206–2.220	2.278, 2.288
	$\mathbf{5}^{3+}$	2.689	99.6, 100.0	74.7, 76.6	2.163–2.216	2.325, 2.338

weaken the Fe–Fe bond, and thus, leading to the significant increase of Fe–Fe distance. In contrast, the HOMOs derived from both BLYP and PBE methods display a δ-bonding feature between iron atoms; note that the overlap between the d orbitals of Fe atoms is very poor (Fig. 10), it is thus expected that the electron occupied this MO contributes very little to the bonding nature between iron atoms. In addition, the p orbitals of S atoms participate in this δ-type HOMO by interacting with the d orbitals of Fe atoms in an antibonding manner. The synergistic effects of the weak Fe–Fe bonding nature and the Fe–S antibonding nature in δ-HOMO lead to slight increase of Fe–Fe distance upon oxidation of $\mathbf{5}^{2+}$. At this stage, we cannot prove which picture, σ- or δ-HOMO, is correct. However, the fact that PBE method reproduces well the crystal structure of $\mathbf{5}^{2+}$ and the geometry changes induced by reduction seems to support the δ-HOMO picture rather than the σ-HOMO picture. It is worth to mention that many hybrid functionals, including the most popular B3LYP, have been shown inadequate to describe transition metal systems, although they give reliable results for main-group organic chemistry [29]. In contrast, pure functionals or hybrid functionals with low percentages of Hartree–Fock exchange give better performance for transition metal chemistry [29]. Therefore, the calculation results support the increase and decrease in the oxidation state from the iron–sulfur core $\{Cp_2Fe_2(\mu\text{-}SEt)_2\}$ complexes both lead to the elongation of Fe–Fe distance.

In summary, the known complex $[Cp_2Fe_2(\mu\text{-}SR)_2(MeCN)_2](PF_6)_2$ (**1**) containing two labile MeCN ligands reacts with 2 equiv. KCN to afford an yellow complex $Cp_2Fe_2(\mu\text{-}SEt)_2(CN)_2$ (**2**). The reaction of complex **2** with equimolar amounts of MeOTf yields a monomethylation product $[Cp_2Fe_2(\mu\text{-}SEt)_2(CN)(CNMe)](OTf)$ (**3**). Dimethylation of complex **2** by 2 equiv MeOTf gives a complex $[Cp_2Fe_2(\mu\text{-}SEt)_2(CNMe)_2](OTf)_2$ (**4**). Complex **1** reacts with dppm, dppa, or dppf, to afford complexes $[Cp_2Fe_2(\mu\text{-}SEt)_2(dppm)](PF_6)_2$ (**5**), $[Cp_2Fe_2(\mu\text{-}SEt)_2(dppa)](PF_6)_2$ (**6**), or $[Cp_2Fe_2(\mu\text{-}SEt)_2(dppf)](PF_6)_2$ (**7**), respectively. The synthesis and characterization of those iron–sulfur core $\{Cp_2Fe_2(\mu\text{-}SEt)_2\}$ complexes have provided fundamental knowledge about iron–sulfur core complexes, necessary for a deeper understanding of the iron–sulfur core enzymes in general.

Acknowledgements

Financial support of the National Science Council (Taiwan) is highly appreciated. We thank the National Center for High-performance Computing for providing computational resources.

Appendix A. Supplementary material

CCDC 685587, 685588, 685589, 685590, 685591, 685592 and 685593 contain the supplementary crystallographic data for **1**–**7**. These data can be obtained free of charge from The Cambridge Crystallographic Data Centre via http://www.ccdc.cam.ac.uk/data_request/cif. Supplementary data associated with this article can be found, in the online version, at doi:10.1016/j.jorganchem.2008.06.025.

References

[1] D. Rickard, G.W. Luther III, Chem. Rev. 107 (2007) 514.
[2] H. Ogino, S. Inomata, H. Tobita, Chem. Rev. 98 (1998).
[3] G.D. Cody, N.Z. Boctor, T.R. Filley, R.M. Hazen, J.H. Scott, A. Sharma, H.S. Yoder Jr., Science 289 (2000) 1337.
[4] C. Huber, G. Waechterhaeuser, Science 281 (1998) 627.
[5] C. Huber, G. Waechterhaeuser, Science 276 (1997) 245.
[6] R.P. Venkateswara, R.H. Holm, Chem. Rev. 104 (2004) 527.
[7] R.H. Holm, P. Kennepohl, E.I. Solomon, Chem. Rev. 96 (1996) 2239.
[8] J.C. Fontecilla-Camps, A. Volbeda, C. Cavazza, Y. Nicolet, Chem. Rev. 107 (2007) 4273.
[9] W.P. Fehlhammer, H. Stolzenberg, in: G. Wilkison (Ed.), Comprehensive Organometallic Chemistry, vol. 4, Pergamon Press, 1982, p. 532.
[10] P. Madec, K.W. Muir, F.Y. Pétillon, R. Rumin, Y. Scaon, P. Schollhammer, J. Talarmin, J. Chem. Soc., Dalton Trans. (1999) 2371.
[11] R. Büchner, J.S. Field, R.J. Haines, J. Chem. Soc., Dalton Trans. (1997) 2403.
[12] R. Büchner, J.S. Field, R.J. Haines, J. Chem. Soc., Dalton Trans. (1996) 3533.
[13] M.T. Toshev, K.B. Dustov, A.I. Nekhaev, G.G. Aleksandrov, S.D. Alekseeva, B.I. Kolobkov, Koord. Khim. 17 (1991) 930.
[14] W. Gaete, J. Ros, R. Yanez, X. Solans, M. Font-Altaba, J. Organomet. Chem. 316 (1986) 169.
[15] R.B. English, Acta Crystallogr., Sect. C 40 (1984) 1567.
[16] G.J. Kubas, P.J. Vergamini, Inorg. Chem. 20 (1981) 2667.
[17] P.J. Vergamini, G.J. Kubas, Prog. Inorg. Chem. 21 (1976) 261.
[18] D.D. Watkins Jr., T.A. George, J. Organomet. Chem. 102 (1975) 71.
[19] J.A.d. Beer, R.J. Haines, R. Greatrex, J. Organomet. Chem. 85 (1975) 89.
[20] P.D. Frisch, M.K. Lloyd, J.A. McCleverty, D. Seddon, J. Chem. Soc., Dalton Trans. (1973) 2268.
[21] J.A.d. Beer, R.J. Haines, R. Greatrex, J.A.v. Wyk, J. Chem. Soc., Dalton Trans. (1973) 2341.
[22] M. Clare, H.A.O. Hill, C.E. Johnson, R. Richards, J. Chem. Soc., Dalton Trans. (1970) 1376.
[23] L.F. Dahl, N.G. Connelly, J. Am. Chem. Soc. 92 (1970) 7472.
[24] G. Ferguson, C. Hannaway, K.M.S. Islam, Chem. Commun. (1968) 1165.
[25] R.B. King, M.B. Bisnette, Inorg. Chem. 4 (1965) 482.
[26] G.J. Kubas, P.J. Vergamini, Inorg. Synth. 21 (1982) 37.
[27] S. Shaik, R. Hoffmann, C.R. Fisel, R.H. Summerville, J. Am. Chem. Soc. 120 (1980) 4555.
[28] Y. Chen, Y. Zhou, J. Qu, Organometallics 27 (2008) 666.
[29] Y. Zhao, D.G. Truhlar, Acc. Chem. Res. 41 (2008) 157.